Mechanical properties of bare and coated soot aggregates probed by atomic force microscopy

Ashoka Karunarathne,[†,¶] Egor V. Demidov,[‡,¶] Ali Hasani,[‡] and Alexei F. Khalizov[*,‡]

†*Otto H. York Department of Chemical and Materials Engineering, New Jersey Institute of Technology, University Heights, Newark, NJ 07102, USA*

‡*Department of Chemistry and Environmental Science, New Jersey Institute of Technology, 323 Dr. Martin Luther King Jr. Blvd, Newark, NJ 07102, USA*

¶*Both authors contributed equally*

E-mail: khalizov@njit.edu

Abstract

Soot from incomplete combustion of carbonaceous materials is a major constituent of atmospheric aerosols. Individual soot particles are aggregates of primary carbon spherules connected together by carbon necks. Freshly released soot aggregates have lacey fractal morphology, but in the atmosphere they undergo compaction, induced by capillary forces exerted by liquid coatings that act against the covalent, cohesive and friction forces between the carbon spherules. Since compaction alters the optical properties and atmospheric lifetime of soot, an ability to model this process is important for predicting the soot's environmental impacts. To inform and validate our recently developed discrete element method (DEM) model of a soot aggregate, we employed force spectroscopy by atomic force microscopy to measure the forces and other mechanical properties related to the bonding between the spherules in the individual soot aggregates. Fractal and compact aggregates, both bare and with liquid coatings were examined. We observed a characteristic sawtooth pattern on force-displacement curves and collected statistics on bonding forces within individual fractal aggregates, as they were fractured and unraveled. Contrary to fractal aggregates, compact aggregates could not be unraveled due to multiple cohesive interactions between spherules. An increase in bonding forces and energies due to capillarity was observed in coated aggregates. The sawtooth pattern was interpreted with the help of a simple conceptual model and the rigorous DEM model was used to show that only one or two necks need to be fractured for a fractal aggregate to yield, and that mechanical failure will most likely be in shear.

Introduction

Atmospheric aerosols affect climate directly by scattering and absorbing light[1] and indirectly by enhancing cloud formation.[2] One of the components of atmospheric aerosols and a strong light absorber is soot,[3] which is produced upon incomplete combustion of carbonaceous materials. Unlike the majority of other atmospheric aerosols, soot particles are not spheres, but aggregates of spheroidal primary carbon particles (monomers) held together by carbon necks. When present in high concentration, these aggregates can coagulate to form agglomerates, which are held together by weaker van der Waals cohesion.[4] While in the atmosphere, soot is subject to aging through a number of processes, including coagulation, surface oxidation, and vapor condensation to form coatings around the aggregates.[5] Capillary forces induced by the liquid coatings cause initially fractal aggregates to become more compact. This compaction changes the optical and transport properties of the aggregates.[6–8] Soot restructuring is controlled by the strength of bonds between monomers that could range from covalent bonding (necking) in the case of nascent soot aggregates to cohesion in the case of agglomerates.[9] Data about the strength of those covalent necked bonds that hold together nascent soot aggregates is scarce.

Rothenbacher et al. performed fragmentation experiments on soot aggregates to evaluate bond strengths through direct impaction.[10] They found that nascent soot aggregates produced by diesel combustion could not be fragmented at all by impaction, which set a lower bound for bond strengths in soot aggregates. Fragmentation was observed only for agglomerates obtained by coagulation of aggregates, and the estimated bonding energies in agglomerates to be 1.2×10^{-16} J. Such agglomerates fragment along the weaker cohesive contacts, while the constituent necked aggregates retain their geometry. Importantly, the fragmentation energy was reduced in the agglomerates subjected to thermal denuding to remove a thin layer of low-volatility hydrocarbon adsorbate, indicating that liquid capillary forces play an important role in addition to cohesive van der Waals forces in binding the monomers.

Another approach to interrogate the mechanical properties of aggregates is force spectroscopy, which is conducted with an atomic force microscope (AFM). Atomic force spectroscopy is a form of tensile testing for nanoscopic samples, which is done by deforming them with a probe and recording the force acting on the probe as a function of displacement.[11] Mechanical properties of aggregates can be obtained by analyzing the features of the force-displacement curves. AFM force-displacement curves of low-dimensional samples typically contain a characteristic sawtooth pattern, which has been observed in protein unfolding experiments,[12,13] force spectroscopy of individual DNA molecules,[14] and indentation of TiO_2 films.[5] The interpretation of the sawtooth-patterned force-displacement curves depends on the nature of samples used in the experiments. Rong et al.[15] performed force spectroscopy on graphitic nanoparticle chain aggregate films (NCA) deposited on a silicon substrate and reported sawtooth patterned force-displacement curves. Such a sample is effectively an agglomerate of aggregates, where the aggregates are held together by van der Waals attraction. The interpretation of the force-displacement curves was that the sawtooth features corresponded to chain rupture and sliding events. In an agglomerated sample, such rupture and sliding events almost certainly occur at weaker cohesive contacts between aggregates rather than at strong covalent bonds corresponding to within individual aggregates.

In this work, we performed force spectroscopy on individual soot aggregates deposited on a silicon substrate to investigate the strengths of fully covalently bonded aggregates as opposed to agglomerates of aggregates held together by cohesion. Consistently with expectations, we observed the characteristic sawtooth pattern in experiments conducted on fresh (low-dimensional) aggregates and only saw a single feature in experiments conducted on compact (high-dimensional) soot globules. We interpreted the features of the sawtooth pattern as shear failure of one or two covalent necks in the aggregate, followed by sliding and creation and breakage of cohesive bonds between the detached aggregate branch and the fragments remaining on the substrate. We corroborated our interpretation of the results with the discrete element method[16] (DEM) model for soot aggregate mechanics by Demidov et al.,[17] which we used to study the distribution of stresses in a deformed aggregate. Results of this study are useful for establishing a procedure for interrogating the structure (dimensionality) of soot aggregates through atomic force spectroscopy and for parametrization of numerical aggregate mechanics models, such as the one by Demidov et al.

Methods

Soot sample preparation

Airborne soot aggregates were generated, size-classified, and aged in a continuous flow system (Fig. 1).[18] Generation was done using an inverted diffusion natural gas burner.[19] Soot aerosol produced by the burner was sampled at 0.3 lpm from the burner using an ejector dilutor operating with particle-free air preheated to 150 °C to avoid water condensation, which after water evaporation could have led to aggregate compaction.[20] Dilution was also crucial to prevent coagulation producing agglomerates of soot aggregates. Diluted sample flow was dried in a Nafion dryer (Perma Pure, PD-07018T-24MSS), leading to a relative humidity (RH) below 5%, as measured by a Vaisala HMM100 sensor. Dry aerosol was passed through a thermal denuder, a steel tube heated to 300 °C, to remove any organic material that could have been formed on particles during combustion, ensuring that the aggregates are "dry". Bare particles were then charge equilibrated with a bipolar ^{210}Po charger (Staticmaster Static Eliminator, 500 μCi) and size-selected to 240 nm electric mobility diameter with a differential mobility analyzer (DMA, TSI 3081A). Monodisperse particles were then either directly collected on silicon wafer chips to obtain samples of bare soot (Fig. 2a) or processed in several ways and then collected to obtain samples of processed soot with different compactness and coating mass fractions (Fig. 2b,2c,2d).

Processing of particles was done by passing the aerosol through a coating chamber - a tubular glass container partially filled with dioctyl sebacate (DOS), a liquid coating material heated to 50 – 80 °C. The aerosol flow became saturated with DOS vapor as it passed through the coating chamber, and upon leaving the chamber and cooling down to room temperature, DOS vapor became supersaturated and condensed on airborne soot aggregates and chamber walls.[18] The amount of condensate was controlled by adjusting the temperature of the coating chamber, with a higher temperature corresponding to a larger coating mass. The mass of condensate present on particles was measured with Aerosol Particle Mass analyzer (APM, Kanomax Model 3601). In some experiments, the coated aerosol was passed through a second

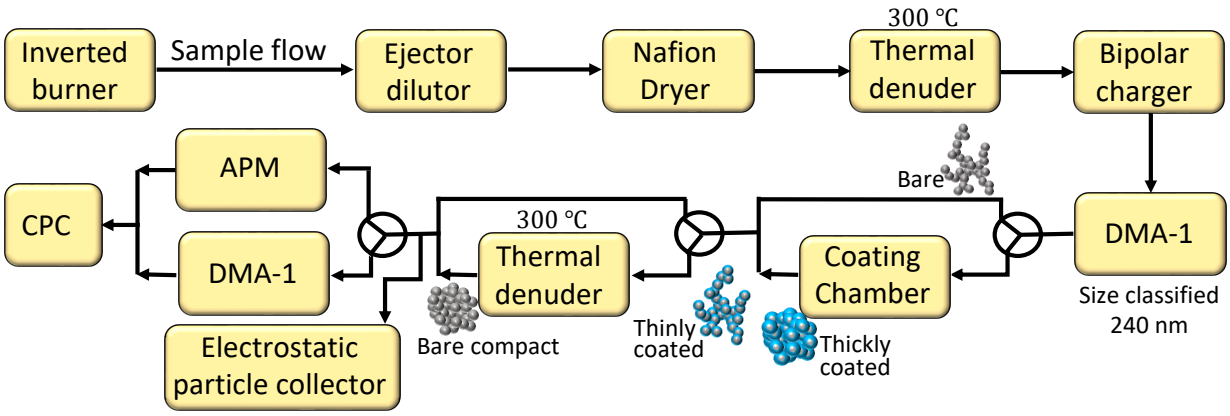

Figure 1: Schematic diagram of the soot sample generation system

thermal denuder maintained at 300 °C to remove DOS coating by evaporation.

Bare and processed soot particles were collected on a silicon substrate (wafer chips from Ted Pella Inc.) with a custom-built electrostatic particle precipitator.[21,22] During particle collection, it was ensured that particles were well separated ($\sim$ 1 particle per 10 μm^2) from each other on the substrate as shown in scanning electron microscope (SEM, JEOL JSM-7900F) images (Fig.2). Particles collected on silicon chips were used in AFM indentation experiments. A matrix of four samples was obtained: bare soot, thinly coated soot (8 % coating by mass), thickly coated soot (71 % coating by mass), and thickly coated-denuded soot. Coated samples that were not denuded retained the liquid coating layer throughout force spectroscopy measurements, which is evident from results presented later in the manuscript and is consistent with the low vapor pressure of DOS (9.69×10^{-6} Pa at room temperature). The coating layers are not visible in SEM images in Fig. 2 due to coating evaporation under the vacuum inside the SEM instrument.

AFM force spectroscopy

Approach-retraction experiments were performed to obtain force curves associated with mechanical deformation of soot aggregates. The experiments were conducted with Bruker's Dimension Icon AFM instrument under ambient conditions. A cantilever with a spring constant of 0.4 N/m was used to measure the force curves at a vertical speed of 1 µm/s. Fig. 3a shows a typical force curve obtained for a bare soot aggregate adhered to a silicon substrate. The dashed black line represents the force acting on the cantilever as the tip approaches the sample, steps (i)-(iii), and solid red line corresponds to the force acting on the tip during stretching of the aggregate, steps (iii)-(v). Zero displacement corresponds to the point where the force switches from compression to tension. A detailed interpretation of the sawtooth pattern is discussed in the following section. Fig. 3b is a SEM image of the AFM tip after the force curve measurements. Presence of soot aggregate fragments on the tip surface confirms the detachment of the aggregate branches from the main aggregate.

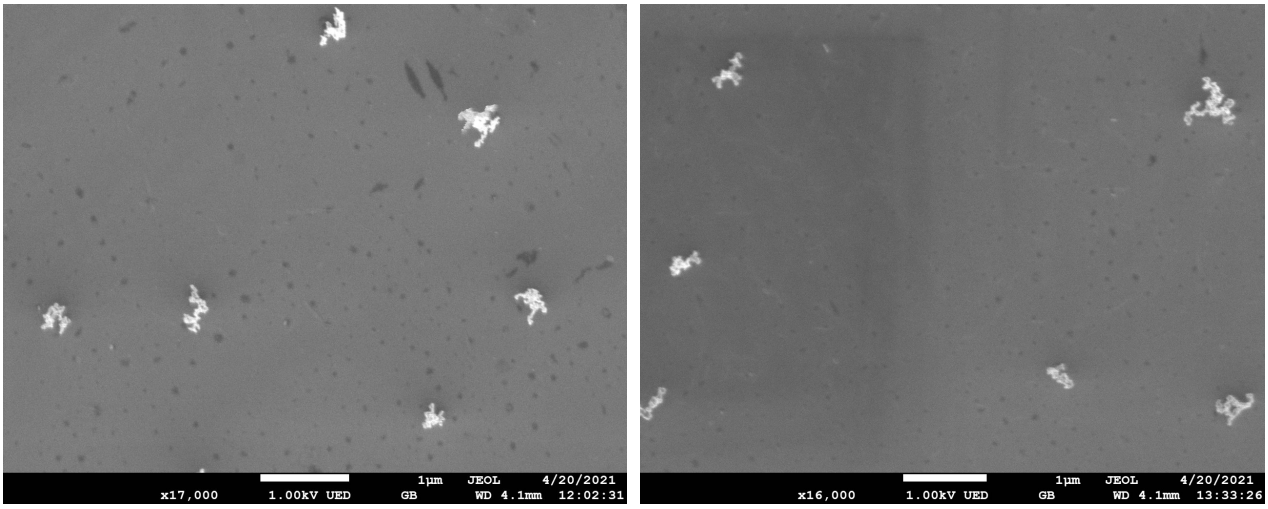

(a) (b)

(c) (d)

Figure 2: SEM images of the soot aggregates collected on silicon substrates: (a) bare (b) thinly coated, (c) thickly coated, and (d) bare compact soot aggregates. The coating cannot be seen on soot aggregates in cases (b) and (c) because DOS was lost by evaporation upon exposure to vacuum in the SEM instrument

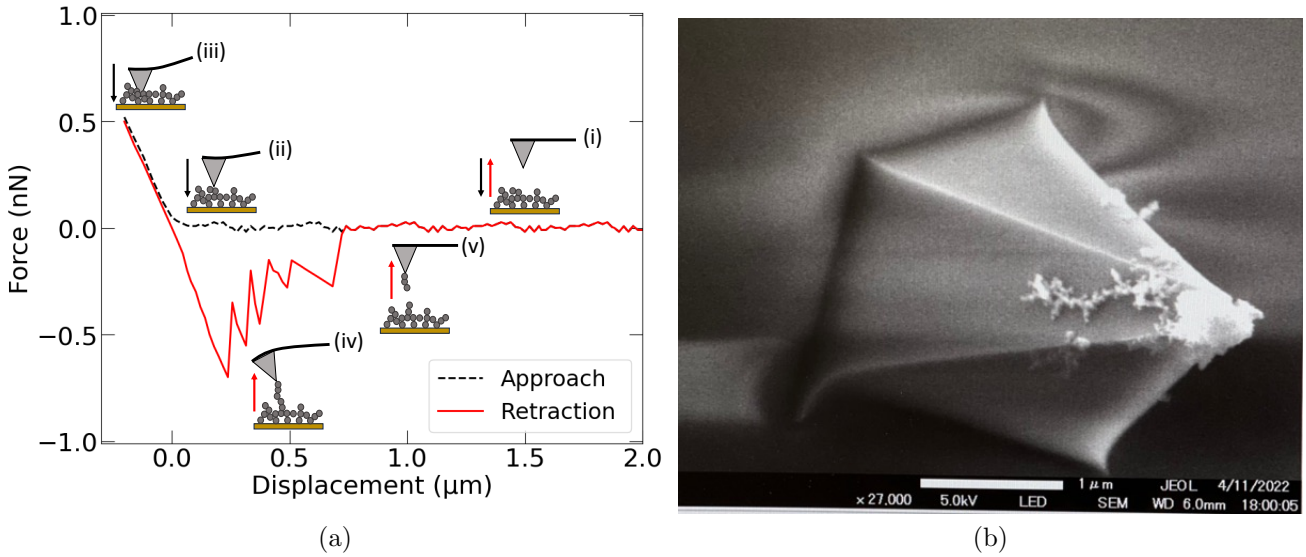

(a) (b)

Figure 3: (a) A typical saw tooth force-displacement curve and an illustration of AFM tip as it: (i) approaches the sample, (ii) contacts the sample, (iii) indents into the sample, (iv) retracts from the sample surface and (v) detaches completely from the sample, (b) SEM image of a AFM tip after the experiments.

Results and discussion

Force curves and their interpretation

Nearly 100 force curves of each sample type (bare, thinly coated, thickly coated and thickly coated-denuded) were measured for statistical analysis of force-displacement curve features. Based on the number of peaks in the sawtooth profile, the most typical force curves for each type of soot aggregates are shown in Fig. 4. All measured force curves for each type of soot are shown in Fig. S1. Force curves with 3 to 6 peaks were observed for bare soot aggregates (Fig. 4a), while 4 to 5 peaks were obtained for thinly coated soot (Fig. 4b). Since the force acting on the tip is negative under tension, by "peaks" we refer to force minima. Force magnitude ranged up to 2 nN for bare and thinly coated soot. The most common feature of the sawtooth profile of these force curves is that the initial peak is the largest in magnitude and subsequent peaks gradually decrease in magnitude. However, several force curves deviate from this behavior having larger intermediate peaks than the first peak. In contrast to bare and thinly coated aggregates, force curves measured for thickly coated compact and bare compact aggregates consisted of a single peak with a significantly larger force ranging from 25 nN to 60 nN in magnitude (Fig. 4c,4d).

We interpret the sawtooth pattern of the force-displacement curves of bare and thinly coated soot as follows: the first peak corresponds to brittle fracture of one or two necks somewhere in the strained aggregate chain. After fracturing, the broken off branch is released and begins sliding up the aggregate (Fig. 5a). As the branch slides, it repeatedly forms frictional-cohesive contacts with monomers in the aggregate that it encounters. To keep sliding, the cohesive contacts need to keep getting broken and reformed. Thus, repeated force

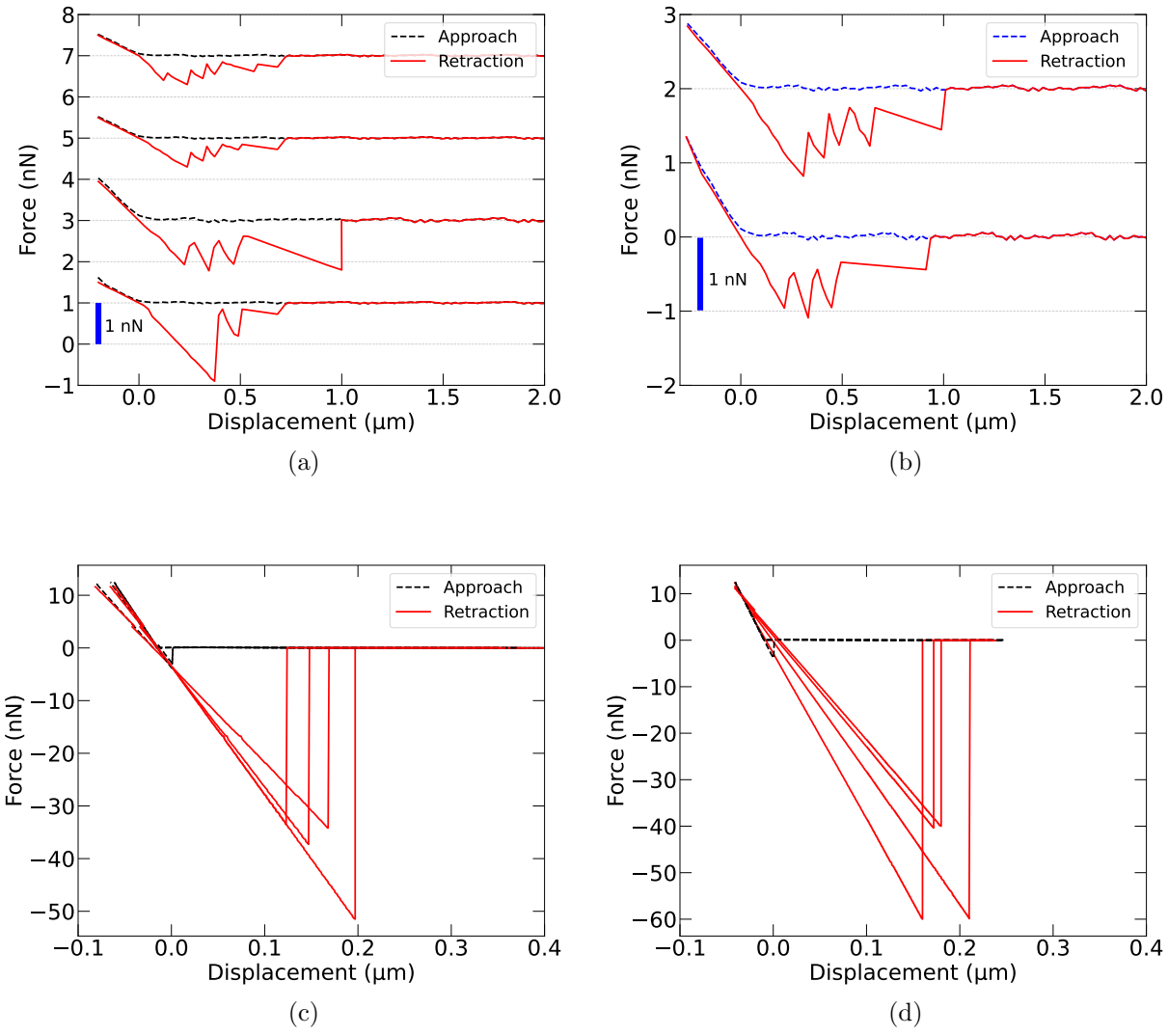

Figure 4: Most typical force curves measured from (a) bare, (b) thinly coated, (c) thickly coated and (d) bare compact soot aggregates.

peaks of decreasing magnitude occur in the force displacement curve (Fig. 5c), consistently with simulations by Demidov et al.[17] Fig. 5c illustrates the state of the aggregate at different points on the force displacement curve. In the figure $F_{\max}$ corresponds to the force needed to sever a neck attaching the aggregate to the branch that is being pulled and ΔF corresponds to the force needed to overcome cohesion between monomers and advance the chain further. The magnitude of cohesion between monomers in contact was estimated using Hamaker equation,[23]

$$F = -\frac{A}{6}\left[\frac{(4r+2\delta)}{(4r+\delta)\delta} - \frac{2}{(2r+\delta)} - \frac{4r^2}{(2r+\delta)^3} - \frac{2r^2(4r+2\delta)}{(4r+\delta)^2\delta^2}\right] \tag{1}$$

where A is the Hamaker constant, a material property which is used to define van der Waals interactions of mesoscopic bodies, r is the radius of a primary particle, and δ is the surface separation between two particles. Since in the limit as σ approaches zero the force becomes infinite, Hamaker equation is usually used down to a surface separation of $0.5 - 1.0$ nm.[24] Fig. 5b shows the profile of van der Waals attractive force between two carbon monomers of radius 15 nm as their surface separation δ is reduced from 20 nm to 0.5 nm. Hamaker constant of $A = 2.55 \times 10^{-19}$ J is assumed.[25] For the range of surface separation from 1 nm to 0.5 nm, the estimated van der Waals force increases from 0.28 nN to 1.2 nN respectively (Fig. 5b inset). These values are consistent with ΔF values seen in Fig. 5c.

The sequence of bond breakage and sliding events can be conceptualized with a system of rupturing parallel springs, where each spring represents the interaction of each monomer in the pulled branch with the main aggregate, as shown in Fig. 5d. The force acting on the spring system with elongation Δx can be determined using Hooke's law,

$$F = -k\Delta x \tag{2}$$

where k is the spring constant, which initially is $k = k_1 + k_2 + k_3$. For simplicity, here we consider identical springs with $k_1 = k_2 = k_3$, assuming identical interaction forces between the monomers in the branch and main aggregate. The force curve determined from the spring system qualitatively simulates the experimental force-displacement pattern.

Contrary to fractal aggregates, there is only one peak on the force-displacement curves in spectroscopy measurements of compact soot aggregates (thickly coated and thickly coated-denuded). In a compact aggregate, the coordination number approaches the random-jammed packing value of 6, which means on average a monomer is in contact with 6 other monomers. This leads to formation of a strong cohesive network which cannot be unraveled by the AFM probe. Instead, the tip elastically deforms the compact globule until adhesion between the globule and the AFM probe is broken and the probe separates leaving the aggregate on the substrate. Thus, the force reduction ΔF from the maximum stretching to complete detachment quantifies the cohesive force between the AFM tip and the surface of the soot aggregate. A detailed analysis of the force-displacement curves for different types of soot aggregates is presented in the following sections.

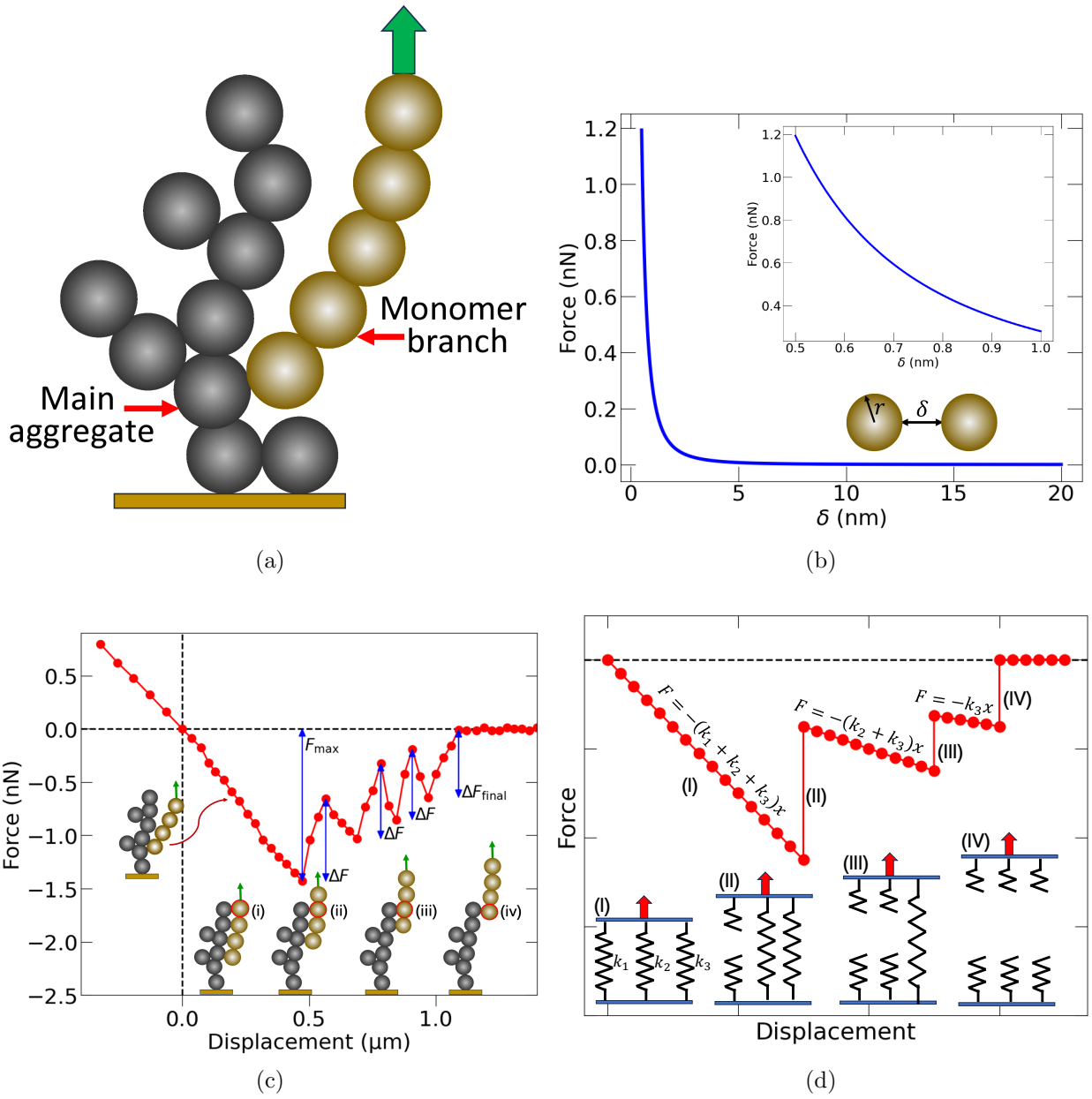

Figure 5: (a) Illustration of a soot aggregate with one of its monomer branches adhering to AFM tip (green arrow), (b) estimated van der Waals attraction between carbon monomers as a function of their separation, (c) physical interpretation of sawtooth patterned force curve and (d) simulated force curve using a spring model.

Bare and thinly coated fractal soot aggregates

Force histograms

Fig. 6 presents the distributions of various force parameters defined in Fig. 5c, $F_{\max}$, ΔF and ΔF_{final} (see Fig. 5c), extracted from nearly 100 force curves of bare and thinly coated soot aggregates. The lines represent log-normal fits for each histogram, their peak positions (mode) and standard deviations, σ are given in Table 1. For both bare and thinly coated soot samples, the neck fracture force, $F_{\max}$ is approximately two to three times higher than ΔF and ΔF_{final}. Initially, the total cohesive force can be weak/negligible, as most of the monomers in the branch are well separated from the main aggregate. However, as the monomer branch breaks off, tilts, and starts to slide along the main aggregate, cohesion becomes stronger, reaching 0.28 – 1.2 nN (Fig. 5b). The value of ΔF, the force drop at every monomer sliding event, is bounded by the above estimate. However, ΔF may represent multiple interactions when the detaching branch interacts with more than one monomer in the main aggregate. The final detachment force, ΔF_{final} is slightly lower than the intermediate detachment forces, ΔF. This supports that ΔF_{final} corresponds to cohesion of a single monomer. All three force parameters are larger in magnitude for thinly coated soot when compared to bare soot, which can readily be explained by additional binding provided by the capillary force induced by the liquid coating. Distributions of $F_{\max}$, and especially ΔF and ΔF_{final} are much more narrow in coated aggregates. This may indicate that the additional binding force is due to capillary menisci of comparable volume rather than from solid-solid interactions, where a higher variability is expected due to deviations of monomers from the ideal spherical shape.

Table 1: The modes (peak positions) and the standard deviations, σ of the log-normal fits of $F_{\max}$, ΔF and ΔF_{final} measured for bare and thinly coated soot aggregates.

Designation	$F_{\max}$ (nN)		ΔF (nN)		ΔF_{final} (nN)	
	Mode	σ	Mode	σ	Mode	σ
Bare	0.74	0.38	0.28	0.64	0.25	0.72
Thinly coated	1.16	0.16	0.58	0.24	0.52	0.28

Displacement histograms

In additions to forces, elongation of soot aggregates at each sliding event can be obtained form the positions of the force curve features (Fig. 7a). The displacement at the initial neck fracturing event is defined as $\Delta x_{\text{initial}}$ between points corresponding to $F = 0$ to $F = F_{\max}$ in the force curve. The displacements of the pulled branch during subsequent sliding events are designated as Δx and the displacement at the final detachment step as Δx_{final}. Histograms of $\Delta x_{\text{initial}}$, Δx, and Δx_{final} for bare and thinly coated soot are shown in Fig. 7b, 7c, 7d respectively. The fitting parameters of the log-normal distributions are given in Table 2. The initial displacements $\Delta x_{\text{initial}}$ of both bare and coated soot aggregates are much higher than the intermediate displacements Δx, because the aggregate needs to be strained more to

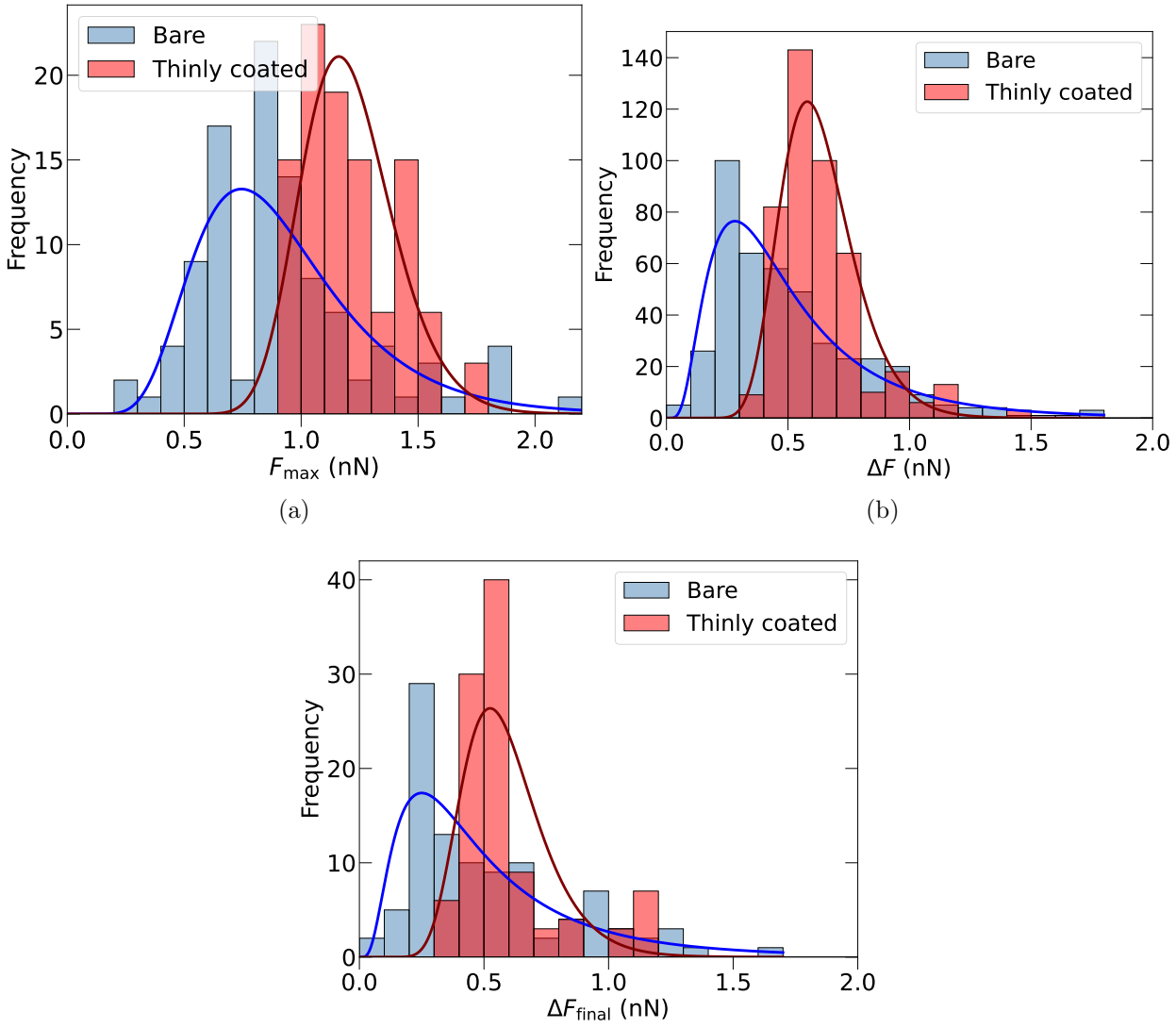

Figure 6: Force histograms of bare and thinly coated fractal soot: (a) maximum force, $F_{\max}$, (b) intermediate detachment forces, ΔF and (c) final detachment force, ΔF_{final}.

reach sufficient tension to sever a neck than to overcome a cohesive contact. Displacements and effective stiffnesses of thinly coated soot are generally slightly higher compared to the bare soot, as the liquid coating provides an additional link between the monomers.[26]

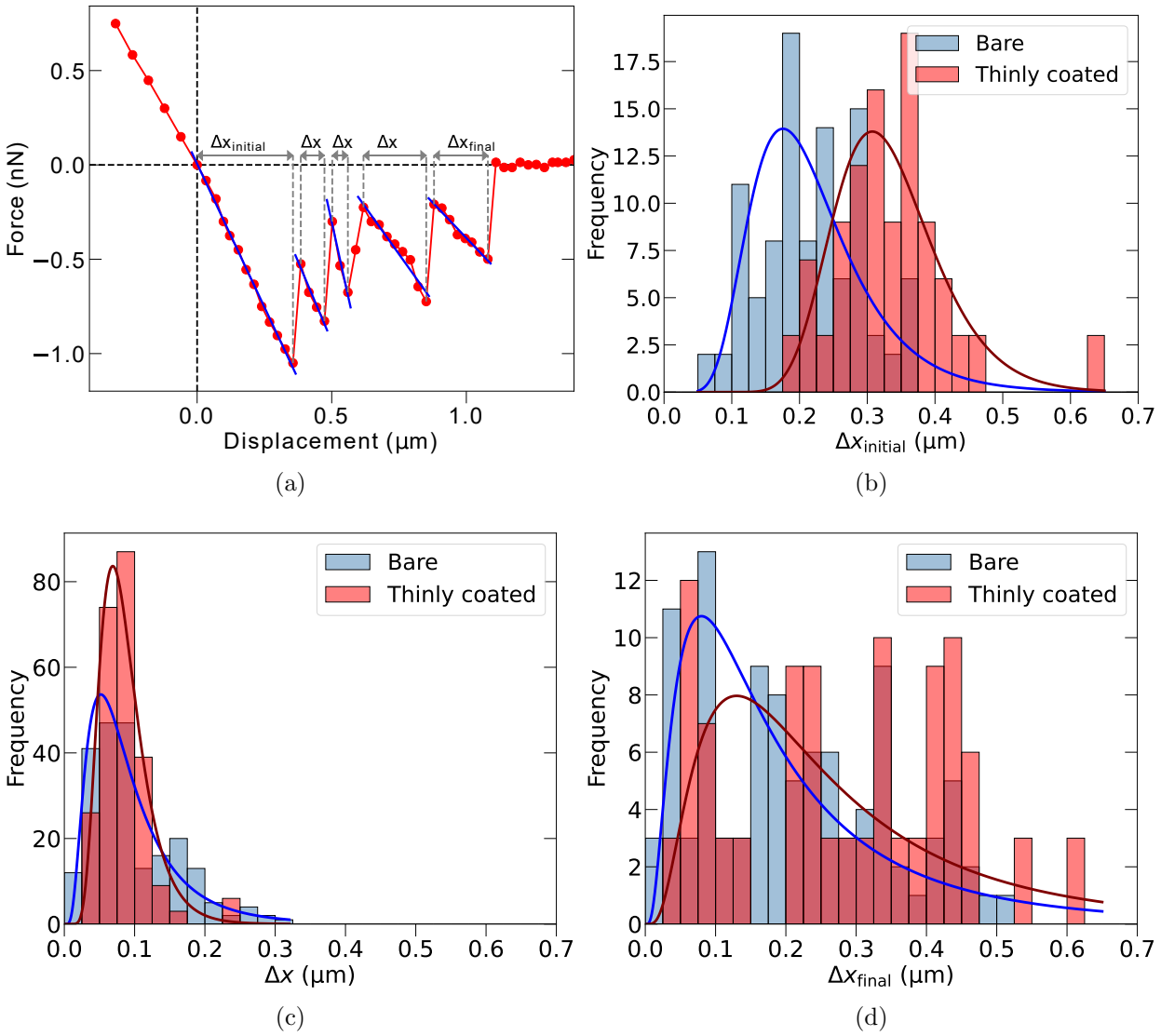

Figure 7: Displacement histograms for bare and thinly coated fractal soot. (a) Displacement and slope measurements from the force curve. Histograms of (b) initial displacement, $\Delta x_{\text{initial}}$, (c) intermediate displacements, Δx, and (d) final displacements,Δx_{final}.

Fragmentation energy histograms

Forces and displacements show significant variability between aggregates. These parameters can be combined to evaluate the mechanical work applied at every step in aggregate breakage and neck sliding process, which is an integrated quantity with expected lower variance. For example, a large force acting over small displacement and a small force acting over large

Table 2: The modes (peak positions) and the standard deviations, σ of the log-normal fits of $\Delta x_{\text{initial}}$, Δx, Δx_{final} measured for bare and thinly coated soot aggregates.

Designation	$\Delta x_{\text{initial}}$ (μm)		Δx (μm)		Δx_{final} (μm)	
	Mode	σ	Mode	σ	Mode	σ
Bare	0.18	0.38	0.05	0.65	0.08	0.83
Thinly coated	0.31	0.23	0.07	0.39	0.13	0.74

displacement may be characterized by similar energies. The total fragmentation energy required for the pulled branch to break off and fully separate from the aggregate, E_{total}, can be determined by computing the area under the entire force curve. The energy of the initial neck breakage, $\Delta E_{\text{initial}}$, intermediate sliding events, ΔE and the final detachment ΔE_{final} are computed by finding the areas under the respective peaks in the force curve.

Overall, there is a clear increase in fragmentation energies for thinly coated soot when compared to those of bare fractal soot aggregates (Fig. 8). The total fragmentation energy of the aggregate, ΔE_{total} ranges from 1.0×10^{-16} to 6.5×10^{-16} J with a log-normal mode of 2.7×10^{-16} J for bare fractal soot. The fragmentation energy increases to ranging from 3.0×10^{-16} to 9.0×10^{-16} J with a log-normal mode of 5.2×10^{-16} J for thinly coated soot. Since the entire branch detachment process involves multiple monomer breakage and sliding events, ΔE_{total} represents the effective bonding energies between all involved monomers, or the mechanical work needed to break off and fully detach a branch.

ΔE_{final} provides an average cohesion energy between two monomers and it ranges from 0.2×10^{-16} – 4.0×10^{-16} J. This bond energy measured from force-displacement curves is in good agreement with average bond energies of 0.5×10^{-16} – 1.2×10^{-16} J measured for airborne diesel soot agglomerates of aggregates in fragmentation experiments.[10] Whereas individually ΔF_{final} and Δx_{final} are spread over a broad range, ΔE_{final} falls in a narrow region indicating an inverse correlation between the force and displacement.

Table 3: The modes (peak positions) and the standard deviations, σ of the log-normal distributions of ΔE_{total}, $\Delta E_{\text{initial}}$, ΔE and ΔE_{final} measured for bare and thinly coated soot aggregates.

Designation	E_{total} (fJ)		$\Delta E_{\text{initial}}$ (fJ)		ΔE (fJ)		ΔE_{final} (fJ)	
	Mode	σ	Mode	σ	Mode	σ	Mode	σ
Bare	0.27	0.38	0.07	0.65	0.03	0.73	0.04	0.68
Thinly coated	0.52	0.23	0.22	0.35	0.08	0.39	0.10	0.49

Modeling of stress distribution in a deformed fractal aggregate

Using the DEM framework for soot aggregate mechanics developed by Demidov et al.,[17] we considered the distribution of neck stresses in a fractal aggregate under load. The goal was to characterize the distribution of stress over the necks in a strained aggregate and to compare

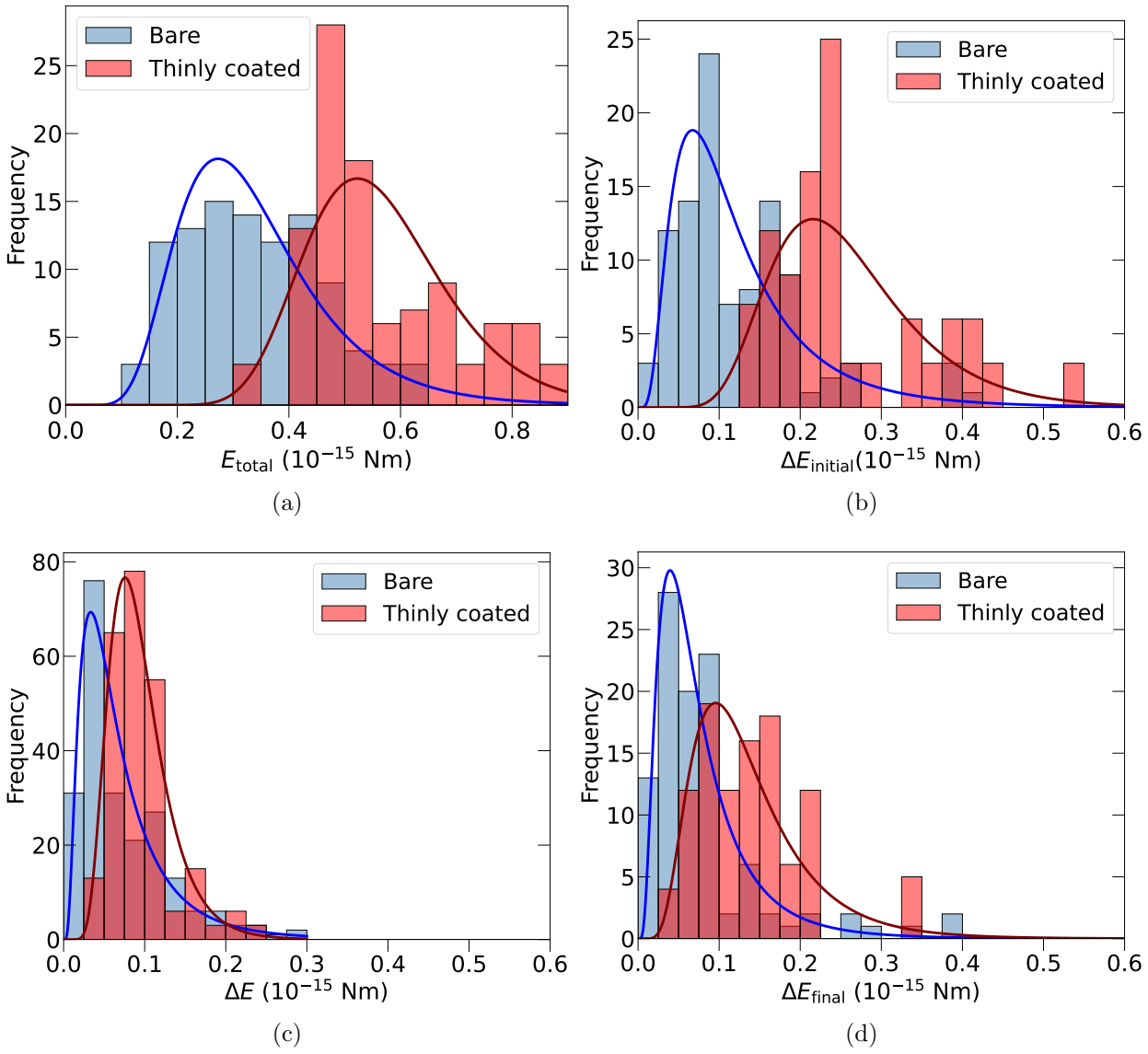

Figure 8: Fragmentation energies of bare and thinly coated soot for (a) entire monomer branch detachment process, E_{total}, (b) initial monomer breakage, $\Delta E_{\text{initial}}$, (c) intermediate breakage/sliding, ΔE and (d) complete detachment ΔE_{final}.

the magnitudes of tensile and shear stresses. A small aggregate was generated with a DEM simulation by filling a 300 nm box with 50 primary particles, each 14 nm in radius r, with randomly directed 1 m/s velocities. Simulations were evolved by time stepping for 5 μs with a step of 500 fs. The rest of the force field parameters (stiffnesses, friction coefficients, etc.) are the same as in the original paper by Demidov et al. Primary particles coagulated into an aggregate with a radius of gyration, R_g, of 111 nm under the influence of van der Waals attraction (Equation 1) and inter-particle friction. This aggregate generation method for DEM mechanics simulations is preferred over other algorithms[27] because it produces aggregates that are at equilibrium with the used force field and the overlap between neighboring particles is minimal, which ensures that any stresses observed during deformation are not caused by inter-particle van der Waals attraction or elastic repulsion of overlapping particles. Soot aggregates follow the fractal scaling law,[28]

$$N = k_0 \left(\frac{R_g}{r} \right)^{D_f} \tag{3}$$

where D_f is fractal dimension and k_0 is the prefactor. Values of D_f and k_0 are known, for fresh combustion soot, to be 1.78 and 1.3 respectively.[8] Thus, our generated aggregate can be validated by calculating its D_f from the given N, R_g, r and the expected value of k_0 and comparing the calculated D_f with the expected value of 1.78. We get $D_f = 1.76$, which is within 2 % error of the expected value and the deviation can be attributed to the random nature of a fractal aggregate.

Elastic necks were inserted between all neighboring primary particles in the generated aggregate, unless addition of a neck would create a cycle in the connected graph formed by particles and necks. As described by Demidov et al.,[17] each neck was modeled with a system of four springs that constrain the four degrees of freedom in a particle pair: normal, tangential, rolling, and torsional. Generated aggregates were deformed by selecting two primary particles that are sufficiently far from each other, highlighted in magenta in Fig. 9a,9c, and applying a 2 nN repulsive force between them. After time stepping to allow the stresses to distribute over the aggregate, potential energies in all springs were recorded. Potential energies of normal springs correspond to tensile stresses in necks. The sum of potential energies of tangential, rolling, and torsional springs correspond to shear stresses in necks. Per-neck distributions of deformation-induced potential energies for tensile and shear components are presented in Figs. 9a,9b and Figs. 9c,9d respectively.

It is clear from Figs. 9a,9b that tensile stresses distribute over necks in a chain of monomers more evenly than shear stresses (Figs. 9c,9d), where most of the stress is concentrated in one or two necks. Moreover, the magnitude of elastic potential energy is much larger in the shear case (by three orders) due to a combination of torques and levers in the aggregate branch. This explains why graphitic necks with large ultimate tensile strength fracture under a relatively low applied force, of the order of $1 - 2$ nN. This also means that under action of either AFM tip or capillary force, necks in a soot aggregate will almost certainly fail in shear and not in tension. Then, only a couple of necks where most of the stress is concentrated will fail and the aggregate will yield. Importantly, energies presented in Fig. 9 are not directly comparable with fracture energies reported in Fig. 8b because these are energies of individual necks, while energies in Fig. 8b include the elastic potential

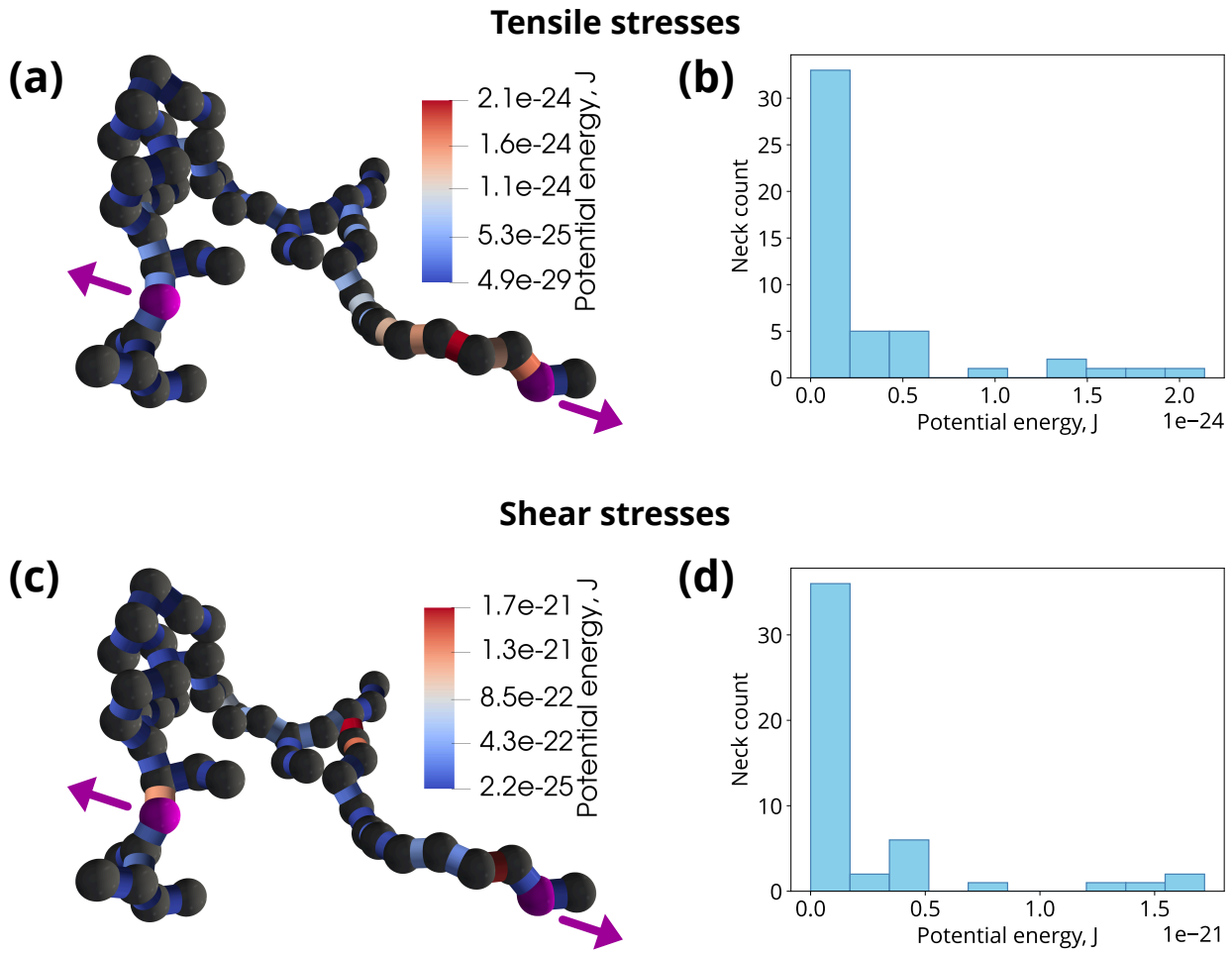

Figure 9: DEM simulations of stress distribution in necks in a fractal aggregate. (a) and (c) show the deformed aggregate, where primary particles to which the deforming force is applied are highlighted in magenta and magenta arrows indicate the direction of the deforming force. Color of the necks is proportional to their elastic potential energy. (b) and (d) show per-neck potential energy distributions. (a) and (b) correspond to tensile deformations. (c) and (d) correspond to shear deformations.

energy of the entire aggregate chain.

Thickly coated and bare compact soot aggregates

Force, displacement and energy histograms

Unlike fractal soot aggregates, both thickly coated and bare compact soot exhibited a single peak on the force-displacement curves. This single peak represents tensile deformation of the aggregate globule followed by a complete detachment of the AFM tip from the aggregate surface. Fig. 10 and Table 4 show the distributions of the associated detachment force, ΔF, displacement, Δx, and energy, E, obtained from the force curves. The detachment forces of both thickly coated and bare compact soot aggregates (25 – 60 nN) are significantly larger than those of fractal soot aggregates ($<$ 2 nN) due to a large number of contact points between a compact globule and the AFM tip. Thus, the detachment force corresponds to cohesion between the AFM probe and the aggregate. Rong et al. found that the detachment force of an AFM tip from a bare silicon substrate was 30 nN,[15] which lies in the range of our measured tip to aggregate adhesive forces. The displacement, Δx ranged up to 0.2 μm while the final displacement, Δx_{final} in fractal soot ranged up to 0.6 μm. This decrease in displacement for the thickly coated and bare compact aggregates confirms that in the compact soot case, the entire aggregate globule is being deformed instead of a single chain being unraveled. This measurement implies that for thickly coated and bare compact soot aggregates, the fragmentation energies should be higher than $\sim 10^{-14}$ J.

Table 4: The modes (peak positions) and the standard deviations, σ of the log-normal fits of ΔF, Δx, dF/dx and E measured for thickly coated and bare compact soot aggregates.

Designation	ΔF (nN)		Δx (μm)		E (fJ)	
	Mode	σ	Mode	σ	Mode	σ
Thickly coated	37.4	0.18	0.17	0.11	3.21	0.25
Bare compact	39.8	0.15	0.17	0.06	3.35	0.20

Conclusions

In this study, statistics of bond and cohesion energies between primary particles in individual soot aggregates were collected experimentally by AFM force spectroscopy. By conducting experiments on individual aggregates, we eliminated the weaker aggregate-aggregate cohesive contacts from our bond energy statistics, focusing on intra-aggregate bonds, which are relevant for restructuring of soot aggregates that did not undergo extensive coagulation. Force spectroscopy is highly suitable for investigation of strong covalent bonds in the aggregates, unlike aerodynamic impaction experiments that would require prohibitively large impact velocities.

We observed the characteristic sawtooth pattern for fractal aggregates, but a single tensile peak for compact aggregates. With the help of a simple conceptual model based on rupturing

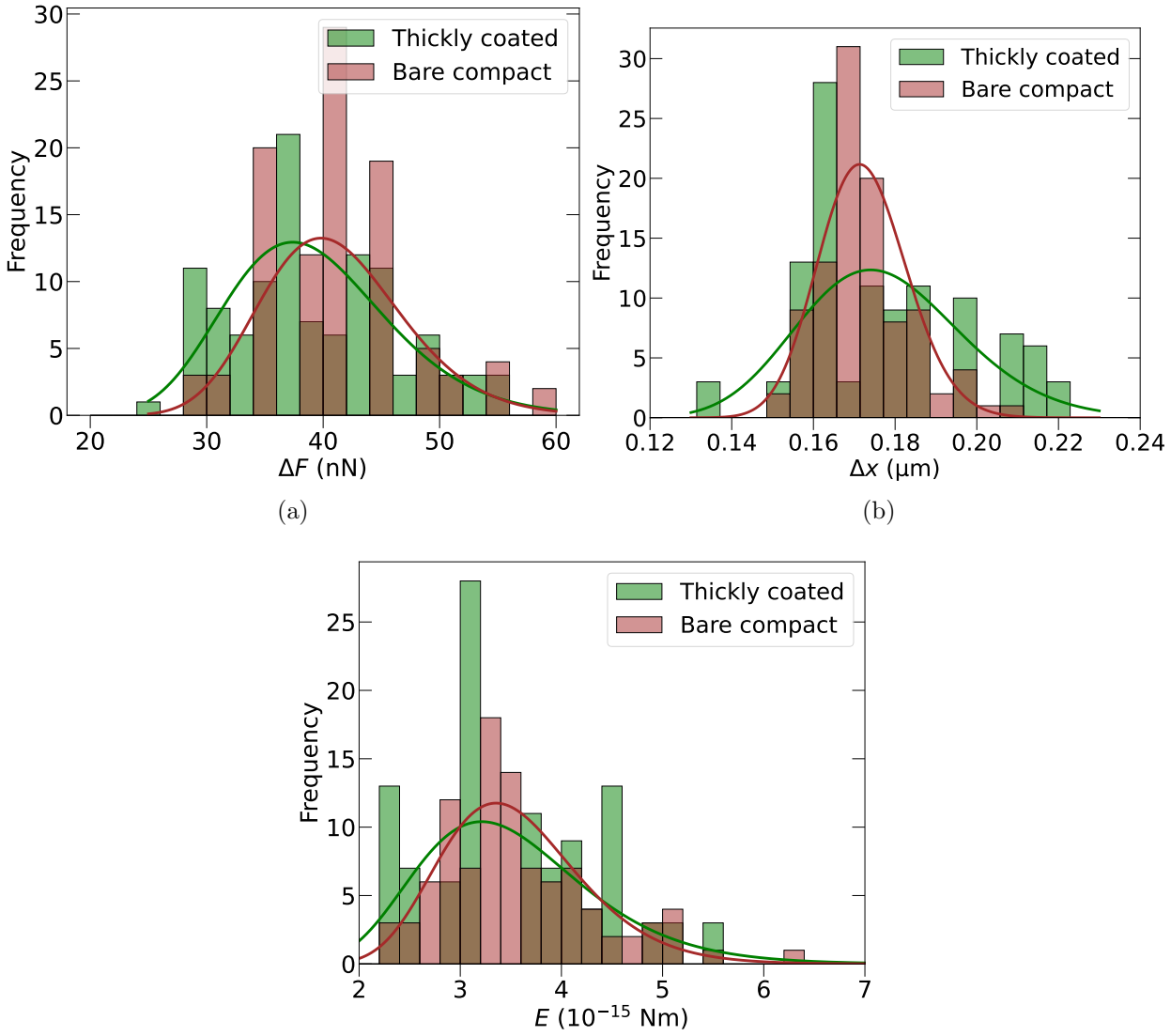

Figure 10: The histograms of (a) Detachment force, ΔF (b) displacement, Δx, and (c) the adhesion energy for thickly coated and bare compact soot aggregates.

springs, the sawtooth pattern was interpreted as shear failure of one or two necks in the strained aggregate chain, followed by repeated cohesion and sliding events occurring between the pulled aggregate branch and the rest of the aggregate. Using a more advanced discrete element method model,[17] we were able to reproduce the characteristic patterns observed during spectroscopy measurements, in terms of both the typical amplitude and number of peaks, validating the model parametrization. This more advanced model supported the interpretation based on the simple conceptual model, showing that most of the stress is focused on a couple of necks and that shear stresses are much higher than tensile stresses (by three orders) due to a combination of torques and levers in a fractal aggregate. The closure between experiments and modeling predictions showcases the discrete element method model as a powerful tool for interpreting and conceptualizing experimental results obtained for granular systems.

Finally, we showed that monomers in compact aggregates are strongly inter-connected with cohesive bonds and cannot be unraveled with AFM force spectroscopy. Instead, they behave as a bulk granular material under mechanical load.

Software availability

Soot aggregates were generated using `SOOT-DEM-GUI` built from git commit `04ab851`, source code available on GitHub. Aggregate deformation simulations were done using `SOOT-DEM` built from git commit `683ec41`, source code available on GitHub. Simulation input files are available in supporting information. Deformed aggregate visualizations were created with `ParaView`.

Acknowledgment

Authors acknowledge the U.S. National Science Foundation award AGS-2222104. AFM spectroscopy experiments were done at Otto H. York center at New Jersey Institute of Technology. We are grateful to Lingfen Rao for AFM instrument training and support.

Author contributions

A.K. - conceptualization, formal analysis, data curation, writing - original draft, visualization; E.V.D - conceptualization, methodology, software, formal analysis, investigation, writing - review and editing, visualization; A.H - investigation; A.F.K - conceptualization, methodology, validation, formal analysis, resources, writing - review and editing, supervision, project administration, funding acquisition.

Appendix A. Supplementary data

A PDF file with all recorded force curves for bare soot, a PDF file with all recorded force curves for thinly coated soot, and a spreadsheet with numeric data used to generate the

histograms are distributed with this article.

References

(1) Chylek, P.; Wong, J. Effect of absorbing aerosols on global radiation budget. *Geophysical research letters* **1995**, *22*, 929–931.

(2) Lohmann, U.; Feichter, J. Global indirect aerosol effects: a review. *Atmospheric Chemistry and Physics* **2005**, *5*, 715–737.

(3) Haywood, J.; Boucher, O. Estimates of the direct and indirect radiative forcing due to tropospheric aerosols: A review. *Reviews of geophysics* **2000**, *38*, 513–543.

(4) Bandyopadhyaya, R.; Lall, A. A.; Friedlander, S. K. Aerosol dynamics and the synthesis of fine solid particles. *Powder Technology* **2004**, *139*, 193–199.

(5) Saathoff, H.; Naumann, K.-H.; Schnaiter, M.; Schöck, W.; Möhler, O.; Schurath, U.; Weingartner, E.; Gysel, M.; Baltensperger, U. Coating of soot and (NH4) 2SO4 particles by ozonolysis products of α-pinene. *Journal of Aerosol Science* **2003**, *34*, 1297–1321.

(6) Sorensen, C. Light scattering by fractal aggregates: a review. *Aerosol Science & Technology* **2001**, *35*, 648–687.

(7) Demidov, E. V.; Enekwizu, O. Y.; Hasani, A.; Qiu, C.; Khalizov, A. F. Differences and similarities in optical properties of coated fractal soot and its surrogates. *Journal of Aerosol Science* **2024**, *180*, 106392.

(8) Sorensen, C. The mobility of fractal aggregates: a review. *Aerosol Science and Technology* **2011**, *45*, 765–779.

(9) Weber, A. P.; Friedlander, S. K. In situ determination of the activation energy for restructuring of nanometer aerosol agglomerates. *Journal of aerosol science* **1997**, *28*, 179–192.

(10) Rothenbacher, S.; Messerer, A.; Kasper, G. Fragmentation and bond strength of airborne diesel soot agglomerates. *Particle and fibre toxicology* **2008**, *5*, 1–7.

(11) Hans-Jürgen Butt, M. K., Brunero Cappella Force measurements with the atomic force microscope: Technique, interpretation and applications. *Surface Science Reports* **2005**, *59*, 1–152.

(12) Rief, M.; Gautel, M.; Oesterhelt, F.; Fernandez, J. M.; Gaub, H. E. Reversible unfolding of individual titin immunoglobulin domains by AFM. *science* **1997**, *276*, 1109–1112.

(13) Oberhauser, A. F.; Hansma, P. K.; Carrion-Vazquez, M.; Fernandez, J. M. Stepwise unfolding of titin under force-clamp atomic force microscopy. *Proceedings of the National Academy of Sciences* **2001**, *98*, 468–472.

(14) Strunz, T.; Oroszlan, K.; Schäfer, R.; Güntherodt, H.-J. Dynamic force spectroscopy of single DNA molecules. *Proceedings of the National Academy of Sciences* **1999**, *96*, 11277–11282.

(15) Rong, W.; Pelling, A. E.; Ryan, A.; Gimzewski, J. K.; Friedlander, S. K. Complementary TEM and AFM force spectroscopy to characterize the nanomechanical properties of nanoparticle chain aggregates. *Nano Letters* **2004**, *4*, 2287–2292.

(16) Cundall, P. A.; Strack, O. D. A discrete numerical model for granular assemblies. *geotechnique* **1979**, *29*, 47–65.

(17) Demidov, E. V.; Gor, G. Y.; Khalizov, A. F. Discrete element method model of soot aggregates. *Preprint (https://arxiv.org/abs/2407.14254), accepted to Physical Review E* **2024**,

(18) Chen, C.; Enekwizu, O. Y.; Fan, X.; Dobrzanski, C. D.; Ivanova, E. V.; Ma, Y.; Gor, G. Y.; Khalizov, A. F. Single parameter for predicting the morphology of atmospheric black carbon. *Environmental science & technology* **2018**, *52*, 14169–14179.

(19) Stipe, C. B.; Higgins, B. S.; Lucas, D.; Koshland, C. P.; Sawyer, R. F. Inverted co-flow diffusion flame for producing soot. *Review of scientific instruments* **2005**, *76*.

(20) Ma, X.; Zangmeister, C. D.; Gigault, J.; Mulholland, G. W.; Zachariah, M. R. Soot aggregate restructuring during water processing. *Journal of Aerosol Science* **2013**, *66*, 209–219.

(21) Chen, C.; Enekwizu, O. Y.; Ma, Y.; Zakharov, D.; Khalizov, A. F. The impact of sampling medium and environment on particle morphology. *Atmosphere* **2017**, *8*, 162.

(22) Dixkens, J.; Fissan, H. Development of an electrostatic precipitator for off-line particle analysis. *Aerosol Science & Technology* **1999**, *30*, 438–453.

(23) Hamaker, H. C. The London—van der Waals attraction between spherical particles. *Physica* **1937**, *4*, 1058–1072.

(24) Ranade, M. Adhesion and removal of fine particles on surfaces. *Aerosol Science and Technology* **1987**, *7*, 161–176.

(25) Tolias, P. Lifshitz calculations of Hamaker constants for fusion relevant materials. *Fusion Engineering and Design* **2018**, *133*, 110–116.

(26) Laube, J.; Baric, V.; Salameh, S.; Mädler, L.; Colombi Ciacchi, L. A new contact model for the discrete element method simulation of TiO nanoparticle films under mechanical load. *Granular Matter* **2018**, *20*, 28.

(27) Filippov, A.; Zurita, M.; Rosner, D. E. Fractal-like aggregates: relation between morphology and physical properties. *Journal of colloid and interface science* **2000**, *229*, 261–273.

(28) Jullien, R. Aggregation phenomena and fractal aggregates. *Contemporary Physics* **1987**, *28*, 477–493.